Near-Infrared Electronic Spectroscopy and Emitting-State Properties of K_2PdCl_4 and K_2PdBr_4

Yanick Pelletier and Christian Reber*

Département de Chimie, Université de Montréal, Montréal, Québec, Canada H3C 3J7

Received April 9, 1996[⊗]

Near-infrared luminescence is observed from single crystals of K_2PdCl_4 and K_2PdBr_4 between 13 500 cm^{-1} and 9000 cm^{-1} (740 nm and 1100 nm). The emission spectrum of K_2PdBr_4 shows vibronic structure involving both the totally symmetrical a_{1g} mode and the non-totally symmetrical b_{1g} mode (D_{4h} point group). The luminescence spectrum of K_2PdCl_4 is less resolved, but shows similar vibronic structure. The maxima of the weak lowest energy absorption bands are at 14 800 cm^{-1} (molar absorptivity = 0.42 M^{-1} cm^{-1}) and 14 645 cm^{-1} (molar absorptivity = 0.38 M^{-1} cm^{-1}) at 8 K for K_2PdCl_4 and K_2PdBr_4, respectively. The Stokes shifts for K_2PdCl_4 and K_2PdBr_4 are 3865 and 3420 cm^{-1}. A gap of approximately 700 (K_2PdCl_4) or 950 cm^{-1} (K_2PdBr_4) separates the emission and absorption spectra. This energy gap and the vibronic structure are analyzed with a model involving the $E_g \times b_{1g}$ Jahn−Teller effect in the ^3E_g excited state of the square-planar $[PdCl_4]^{2-}$ and $[PdBr_4]^{2-}$ complexes. The Huang−Rhys parameters $S_{a_{1g}}$ and $S_{b_{1g}}$ are 6.7 and 0.2 for K_2PdCl_4, leading to bond elongations of 0.12 Å for each of two opposing Pd−Cl bonds and of 0.09 Å for each of the other two bonds. The corresponding values for K_2PdBr_4 are 7.6 ($S_{a_{1g}}$), 0.4 ($S_{b_{1g}}$), 0.12 Å, and 0.07 Å.

Introduction

Square-planar transition metal complexes were among the first coordination compounds to be discovered, and their molecular and crystal structures have been characterized in detail.[1,2] A common structural feature of many square-planar compounds of platinum(II) are one-dimensional stacks of chromophores oriented with their 4-fold axis parallel to the crystallographic *c*-axis. Interactions between the metal centers along this axis have been studied in detail for tetracyanoplatinates.[3] Tetrahaloplatinate(II) complexes and their derivatives are well-studied representatives of this coordination geometry with interesting spectroscopic properties.[4−16] Some of the isostructural halides of palladium(II) have been known for more than 150 years,[17] but their electronic spectra have received much less attention than those of the platinum analogs.[18,19] Emission spectra or luminescence lifetime measurements have been reported only for a limited number of palladium(II) complexes.[8,20,21] Luminescence from palladium(II) in the solid state is observed in the near-infrared (near-IR) spectral region, not routinely accessible to standard luminescence spectrometers, and therefore only approximate band maxima[8] or incomplete spectra[20] have been published. The tetragonal crystal structure[22,23] and the high D_{4h} symmetry of the square-planar $[PdX_4]^{2-}$ molecular units make these complexes very attractive from a spectroscopic perspective.

Our main goal is to characterize the lowest energy excited electronic states of the title compounds. The resolved low-temperature luminescence and absorption spectra show two unusual features. First, the vibronic structure of the emission spectra contains transitions involving a non-totally symmetrical vibrational mode. Second, the emission and absorption spectra reveal an energy gap of up to 950 cm^{-1} between the onset of the absorption and luminescence bands. The low-energy electronic transitions are assigned with a standard ligand-field model from the literature[6] and confirm the existing ligand-field assignments for the higher energy excited states of the title compounds.[10] We use the time-dependent theory of spectroscopy to rationalize both the vibronic structure in the luminescence spectra and the observed energy gap with a set of two-dimensional potential energy surfaces for the ground and emitting states. Finally, we compare the emitting-state properties of the title compounds to those of their platinum analogs, illustrating the differences between these structurally related materials.

Transition metal ions in halide and oxide environments have been the focus of much recent interest as solid-state laser materials because of their intense, broad-band near-IR luminescence bands.[24,25] Second-row ions, such as palladium(II),

[⊗] Abstract published in *Advance ACS Abstracts,* January 1, 1997.

(1) Werner, A. *Z. Anorg. Allg. Chem.* **1893**, *3*, 267.
(2) Dickinson, R. G. *J. Am. Chem. Soc.* **1922**, *44*, 2404.
(3) Gliemann, G.; Yersin, H. *Struct. Bonding* **1985**, *62*, 87.
(4) Martin, D. S. *Inorg. Chim. Acta, Rev.* **1971**, *5*, 107.
(5) Patterson, H. H.; Godfrey, J. J.; Kahn, S. M. *Inorg. Chem.* **1972**, *11*, 2872.
(6) Francke, E.; Moncuit, C. *Theor. Chim. Acta* **1973**, *29*, 319.
(7) Moncuit, C. *Theor. Chim. Acta* **1975**, *39*, 255.
(8) Tuszynski, W.; Gliemann, G. *Z. Naturforsch.* **1979**, *34a*, 211.
(9) Yersin, H.; Otto, H.; Zink, J. I.; Gliemann, G. *J. Am. Chem. Soc.* **1980**, *102*, 951.
(10) Vanquickenborne, L. G.; Ceulemans, A. *Inorg. Chem.* **1981**, *20*, 796.
(11) Chang, T.-H.; Zink, J. I. *J. Am. Chem. Soc.* **1984**, *106*, 287.
(12) Chang, T.-H.; Zink, J. I. *Inorg. Chem.* **1985**, *24*, 4499.
(13) Chang, T.-H.; Zink, J. I. *Inorg. Chem.* **1986**, *25*, 2736.
(14) Phillips, J. R.; Zink, J. I. *Inorg. Chem.* **1986**, *25*, 1503.
(15) Reber, C.; Zink, J. I. *J. Phys. Chem.* **1991**, *95*, 9151.
(16) Bridgeman, A. J.; Gerloch, M. *Mol. Phys.* **1993**, *79*, 1195.
(17) Berzelius, J. J. *K. Sven. Vetenskapsakad. Handl.* **1828**, 45.
(18) Francke, E.; Moncuit, C. *C. R. Seances Acad. Sci., Ser. B* **1970**, *271*, 741.
(19) Rush, R. M.; Martin, D. S.; LeGrand, R. G. *Inorg. Chem.* **1975**, *14*, 2543.
(20) Güntner, W.; Gliemann, G.; Kunkely, H.; Reber, C.; Zink, J. I. *Inorg. Chem.* **1990**, *29*, 5238.
(21) Oetliker, U.; Güdel, H. U. *J. Lumin.* **1993**, *58*, 350.
(22) Mais, R. H.; Owston, P. G.; Wood, A. M. *Acta Crystallogr.* **1972**, *B28*, 393.
(23) Martin, D. S.; Bonte, J. L.; Rush, R. M.; Jacobson, R. A. *Acta Crystallogr.* **1975**, *B31*, 2538.
(24) Jacobsen, S. M.; Tissue, B. M.; Yen, W. M. *J. Phys. Chem.* **1992**, *96*, 1547.
(25) Brunold, T. C.; Hazenkamp, M. F.; Güdel, H. U. *J. Am. Chem. Soc.* **1995**, *117*, 5598.

S0020-1669(96)00388-6 CCC: $14.00

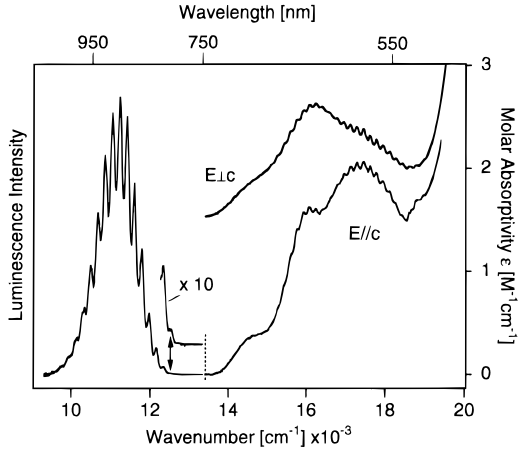

Figure 1. Single-crystal luminescence and polarized absorption spectra of K_2PdBr_4 at 8 K. The vertical dotted line separates emission and absorption spectra.

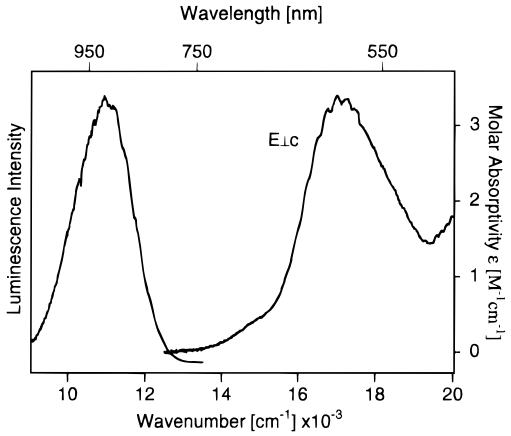

Figure 2. Low-temperature single-crystal emission and absorption spectra of K_2PdCl_4 at 8 K in the same wavenumber range as for Figure 1.

have received less attention for such applications, another important reason motivating our spectroscopic study of the title compounds.

Experimental Section

Crystals for spectroscopic measurements were obtained by slow evaporation of saturated solutions of the title compounds in ethanol/water (60/40 v/v) at room temperature over a period of weeks. Starting materials were obtained from Strem Chemicals. All samples were maintained in a desiccator containing concentrated solutions of HCl and HBr for K_2PdCl_4 and K_2PdBr_4, respectively. In addition, we have synthesized K_2PdCl_4 and K_2PdBr_4 from PdO using literature procedures.[19] The electronic spectra of these crystals and those of the recrystallized commercial compounds are identical. Our experimental conditions are similar to those used in the structural studies of both title compounds.[22,23] We cannot exclude the formation of the dihydrate $K_2PdBr_4 \cdot 2H_2O$, whose crystal absorption spectra are reported to be identical to those of K_2PdBr_4.[8]

Absorption Spectra. The optical quality of the sample crystals was examined under a microscope between crossed polarizers, and extinction directions were determined. The thickness of the samples for which spectra are reported was 230 μm for K_2PdCl_4 and 620 μm for K_2PdBr_4. The samples were mounted in a helium gas-flow cryostat (Oxford Instruments CF 1204), and low-temperature polarized spectra were measured on a Varian Instruments Cary 5E spectrometer.

Emission Spectra. Single crystals or polycrystalline samples of K_2PdCl_4 and K_2PdBr_4 were cooled in the helium gas flow cryostat. A 150 W Xe arc lamp filtered through a copper sulfate solution and a Schott BG18 filter was used as excitation source. The spectra were recorded with a Spex 1800-II 0.75 m monochromator, a cooled Hamamatsu R406 photomultiplier, and a lock-in amplifier. All luminescence spectra are unpolarized and were corrected for system response. This is especially important for the wavelength range of the title compounds, since detector sensitivities vary greatly between 750 and 1100 nm. A detailed description of the instrumentation and the correction procedures is given in ref 26.

Luminescence Lifetimes. Samples were cooled to low temperature and excited with the 308 nm line of a XeCl excimer laser. The laser power did not exceed 5 mJ/pulse measured at the exit window of the laser. The time-dependent luminescence signal was dispersed by a Spex 500M 0.5 m monochromator set to a spectral band width of 3.2 nm and detected by a cooled Hamamatsu R406 photomultiplier and a digital oscilloscope.[26]

Spectroscopic Results

The luminescence and polarized absorption spectra of K_2PdBr_4 at 8 K show well-resolved vibronic structure, as illustrated in Figure 1. The lowest energy absorption band has comparable intensity in both polarizations, in contrast to the platinum analogs of the title compounds, where the lowest energy band is predominantly polarized perpendicular to the crystallographic *c* axis, which coincides with the 4-fold axis of the square-planar complexes.[8] The overall shape of the low-energy absorption bands in Figure 1 is also different from the corresponding bands of K_2PtBr_4.[8] The highest energy maximum in the luminescence spectrum is at 12 525 cm^{-1}, indicated by the arrow in Figure 1. Unresolved spectra are observed at temperatures above 70 K. Positions and relative intensities of the vibronic peaks do not change significantly between 8 and 70 K. The onset of the first absorption band begins at 13 580 cm^{-1}, higher in energy by 950 cm^{-1} than the onset of the luminescence spectrum. The maximum of the emission band is at 11 225 cm^{-1} and shows a vibronic progression with a separation of 184 $\pm$ 3 cm^{-1} between its members, close to the a_{1g} vibrational frequency of 187.4 cm^{-1}.[27] Each vibronic peak shows shoulders, and the shape of the peaks changes along the progression.

We observed an unresolved luminescence spectrum from $[PdBr_4]^{2-}$ in a low-temperature glass (ethanol/water, 95/5 v/v) at 8 K with a band maximum at 10 520 cm^{-1} and a width of approximately 840 cm^{-1}, compared to 11 225 and 1000 cm^{-1} for the neat crystal. These similarities of the luminescence spectra from different environments indicate only small spectroscopic effects resulting from interactions between square-planar chromophores in the crystals. No luminescence was observed for $[PdCl_4]^{2-}$ in a low-temperature glass.

Three resolved absorption bands in the visible and near-IR can be distinguished in Figure 1. Their maxima are at 14 645, 16 035, and 17 420 cm^{-1}, and the two higher energy bands have a resolved progression of 165 $\pm$ 2 cm^{-1} in both E $\parallel$ c and E $\perp$ c polarizations. The lowest energy band was not reported in the literature,[8,19] most likely because of its very low intensity. For the higher energy bands, we observe polarizations and molar absorptivities very similar to the literature results.[8,19] The Stokes shift of K_2PdBr_4 obtained from the lowest energy absorption maximum and the emission maximum is 3420 cm^{-1}, smaller by 30% than the Stokes shift of the platinum analog.[8]

Figure 2 shows single-crystal luminescence and absorption spectra of K_2PdCl_4 measured at 8 K. The highest energy peak is at 12 735 cm^{-1}, higher by 210 cm^{-1} than for K_2PdBr_4. An energy gap of approximately 700 cm^{-1} separates luminescence and absorption spectra, a smaller difference than for K_2PdBr_4. The luminescence band maximum is at 10 935 cm^{-1}, and a progression of 300 $\pm$ 9 cm^{-1} is observed.

(26) Davis, M. J.; Reber, C. *Inorg. Chem.* **1995**, *34*, 4585.

(27) Bosworth, Y.; Clark, R. J. H. *Inorg. Chem.* **1975**, *14*, 170.

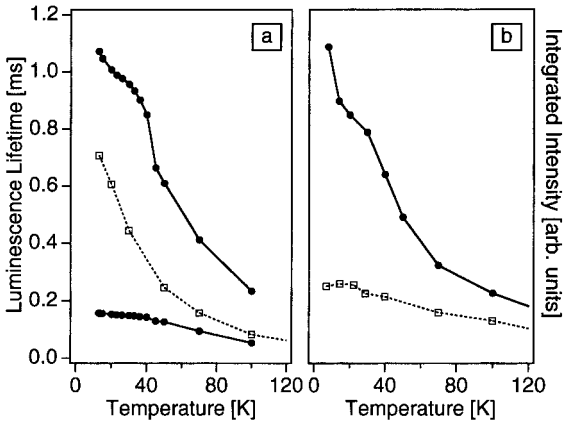

Figure 3. (a) Luminescence lifetimes at 890 nm for K_2PdBr_4 (double exponential, solid circles) and for K_2PdCl_4 (single exponential, open squares) as a function of temperature. (b) Integrated luminescence intensities as a function of temperature for K_2PdBr_4 (solid circles) and for K_2PdCl_4 (open squares).

The absorption spectrum shows low-energy band maxima at approximately 14 800 and 17 005 cm^{-1}. A progression of 257 $\pm$ 5 cm^{-1} is observed on the latter band in E $\perp$ c polarization. The other polarization does not show resolved vibronic structure for any of the bands. Again, the first absorption band is unresolved and was not reported in the literature[8,18,19] due to its low intensity. The molar absorptivities and polarizations of the higher energy bands are identical to those in the literature.[8,18,19] The luminescence and absorption spectra for K_2PdCl_4 in Figure 2 are in very good agreement with the literature emission and excitation spectra.[21] The maximum of the lowest energy excitation band is reported at approximately 15 300 cm^{-1},[21] confirming the low-energy absorption band in Figure 2. The Stokes shift is 3865 cm^{-1}, again smaller than the Stokes shift of 5000 cm^{-1} for K_2PtCl_4.[8]

We doped K_2PdCl_4 into K_2PtCl_4, a host lattice with structured emission at higher energy,[9,28] in an unsuccessful attempt to improve the resolution of the luminescence spectrum for $[PdCl_4]^{2-}$. At a concentration of 0.1% Pd^{2+}, both the steady-state and time-resolved luminescence spectra are a superposition of an emission identical to pure K_2PtCl_4 and a poorly resolved K_2PdCl_4 band.

Figure 3 shows luminescence lifetimes and intensities as a function of temperature for K_2PdBr_4 and K_2PdCl_4. The lifetimes in Figure 3a were obtained at 890 nm, a wavelength close to the maxima of the emission bands of both title compounds. The lifetimes of K_2PdBr_4 at 850 and 940 nm differ by less than 5% from the values obtained at 890 nm. All decay curves for K_2PdBr_4 show a double-exponential behavior between 13 and 100 K. At 30 K, the long lifetime is 960 μs (890 nm) and accounts for 83% of the total intensity. The short lifetime is 150 μs, accounting for only 17% of the total intensity. Both lifetimes are shown in Figure 3a as solid symbols. Luminescence decay measurements at 12 500 $\pm$ 60 cm^{-1}, in the region of the highest energy luminescence peak, also lead to double-exponential decay curves. The relative contributions of the long and short lifetimes remain constant at a ratio of 4/1 over a change in laser power by almost 2 orders of magnitude. Likely origins of the weak, short-lived emissions are square-planar luminescent centers in a slightly irregular environment, e.g., at the crystal surfaces.

Experimental evidence that the luminescence spectra arise from the intrinsic square-planar chromophores and not from a minority of emitting traps includes the observation of identical spectra obtained with crystals grown from different starting materials and using different syntheses, the relatively small Stokes shifts compared to those of the platinum analogs, and the similar band position obtained in a low-temperature glass, where energy-transfer processes to traps can be ruled out. Efficient energy transfer processes to emitting traps in the crystals are not likely to dominate the luminescence behavior, based on lifetime measurements on K_2PtCl_4 doped with $[PdCl_4]^{2-}$. In these systems, the tetrachloropalladate ions act as intentional traps. The doped crystals show luminescence from both the majority $[PtCl_4]^{2-}$ (band maximum at 12 900 cm^{-1}) and $[PdCl_4]^{2-}$ (10 935 cm^{-1}). The 13 K luminescence lifetime measured on a sample containing 4% $[PdCl_4]^{2-}$ is 90 μs at 12 900 cm^{-1}, much longer than the rise time of less than 3 μs measured for the $[PdCl_4]^{2-}$ emission at 10 935 cm^{-1}. These two times are identical if the luminescence behavior is determined by efficient energy transfer to traps, but in our experiments they differ by more than a factor of 30.

Radiative lifetimes were calculated from the oscillator strength of the lowest energy absorption band. A least-squares analysis of the lowest energy bands in Figure 1 with Gaussian band shapes[29] leads to an oscillator strength of 1.2×10^{-6}. The corresponding radiative lifetime is 1.6 ms, assuming an electric dipole mechanism[30] and refractive indices of 1.5804 and 1.5389 for K_2PdBr_4 and K_2PdCl_4, respectively.[19] This calculated lifetime compares favorably to the experimental lifetime of 1.07 ms at 13 K for the majority luminophore in crystalline K_2PdBr_4, further experimental evidence indicating that the luminescence arises from the unperturbed molecular units.

The luminescence lifetimes of K_2PdCl_4 show a steady decrease with temperature, as illustrated in Figure 3a. At 30 K, we determine luminescence lifetimes of 450 μs at 890 nm, near the band maximum, and 460 μs at 980 nm, again showing only small variations with wavelength. All luminescence decay curves for K_2PdCl_4 are single exponential. The radiative lifetime calculated from the oscillator strength of 1.0×10^{-6} is 2.9 ms, longer than the low-temperature experimental value of 0.7 ms at 13 K, indicating a lower quantum yield for K_2PdCl_4 than for K_2PdBr_4.

The integrated luminescence intensities for both title compounds decrease with increasing temperature, as illustrated in Figure 3b. The higher absolute luminescence intensities for K_2PdBr_4 than for K_2PdCl_4 are most likely due to the more intense absorption bands of K_2PdBr_4 in the wavelength range of our excitation source. Both the luminescence intensity and the lifetime of K_2PdBr_4 as a function of temperature show a shoulder near 30 K, not observed for K_2PdCl_4. A possible reason for this deviation from a steady decrease is the Boltzmann population of levels with shorter lifetimes than the low-temperature emitting state, corresponding to different levels of the ^3E_g excited state, which is split by spin−orbit coupling. The shoulder at 30 K is likely to result from the thermal population of a level higher in energy by less than 10 cm^{-1} than the emitting state, with the steeper decrease at temperatures above 30 K arising from the population of a much shorter-lived third level higher in energy by at least 50 cm^{-1}. Similar models were successfully used for the analysis of luminescence decay rates in the literature.[31] The strong temperature dependence of the luminescence intensity for the title compounds underlines the importance of nonradiative relaxation processes. We do not attempt a detailed analysis of the temperature-dependent relax-

(28) Preston, D. M.; Güntner, W.; Lechner, A.; Gliemann, G.; Zink, J. I. *J. Am. Chem. Soc.* **1988**, *110*, 5628.
(29) Pelletier, Y.; Reber, C. *Can. J. Chem.* **1995**, *73*, 249.
(30) Imbusch, G. F. In *Luminescence Spectroscopy*; Lumb, M. D., Ed.; Academic Press: London, New York, 1978; p 1.
(31) Crosby, G. A.; Hager, G. D.; Hipps, K. W.; Stone, M. L. *Chem. Phys. Lett.* **1974**, *28*, 497.

ation rates and luminescence intensities in Figure 3 because of the prohibitive number of parameters needed in a quantitative model.

For both title compounds, the same temperature dependence of the luminescence intensity was observed with three different samples. Luminescence lifetime measurements on a second sample lead to rates differing by less than 4% from the values in Figure 3a.

Discussion

Ligand-Field Assignments. Overall absorption spectra of both tetrahalopalladates and tetrahaloplatinates have been reported, and assignments have been made for the bands in the visible and UV regions.[4,8,18,19] The square-planar complexes have exact D_{4h} point group symmetry and tetragonal crystal structures isomorphous to K_2PtCl_4 and K_2PtBr_4 (space group $P4/mmm$).[22,23] The lattice parameters for K_2PdCl_4 differ by less than 0.05 Å from those of K_2PtCl_4.[22] All square-planar molecular units of the title compounds are equivalent in this structure.

We use the ligand-field matrix for square-planar d^8 systems in ref 6 to assign the low-energy absorption bands presented in Figures 1 and 2. The angular overlap and Racah parameters given for the title compounds in ref 10 were used as a starting point, and mixing between the 5s and $4d_{z^2}$ orbitals of the metal center was allowed. We used the parametrization scheme of ref 6 and orbital mixing parameters $a = a_0 = b = 0$, corresponding to a stabilization of the $4d_{z^2}$ orbital through mixing with the 5s orbital by an energy equivalent to the destabilization of the $4d_{z^2}$ orbital by σ metal−ligand interactions. This choice of parameters is identical to $\sigma_{sd} = \sigma$ in ref 10, an s−d interaction found empirically to hold for a series of square-planar d^8 and d^9 compounds.

We increase e_σ by 4% for K_2PdBr_4 and by 2% for K_2PdCl_4 to reproduce the positions of the calculated low-energy band maxima. The Racah parameter B for both title compounds is reduced to 64% of the free ion value of 826 cm^{-1} for palladium(II),[32] and a C/B ratio of 4.2 was used. These interelectronic repulsion parameters are in the usual range for a variety of transition metal compounds[33] and identical to those in ref 10. The agreement between observed and calculated band maxima is satisfactory, as seen from the comparison of all calculated energies and the experimental band maxima in Table 1. Another recently published set of ligand-field parameters[16] involves a reduction of B to 12% of the free ion value and a C/B ratio of 21, possibly a manifestation of nonspherical electron repulsion parameters. This effect has been studied in detail for tetragonal chromium(III) complexes,[34] but the total number of observed transitions for the title compounds does not allow a rigorous determination of the necessary additional parameters. We limit our analysis for the title compounds to the standard Racah parameters in the usual numerical range. Other differences between the model used for the calculations in Table 1 and the model in ref 16 were discussed recently.[35]

The lowest energy excited state for both title compounds is ^3E_g, split by spin−orbit coupling into four nondegenerate and one doubly degenerate level. We do not observe the individual levels in our spectra, and therefore the spin−orbit coupling constant ζ for the ^3E_g state cannot be determined from our experimental data. It is likely to be significantly reduced from its free-ion value of 1412 cm^{-1} for palladium(II)[32] by Ham quenching in this orbitally degenerate state.[36−39] The temperature dependence of the luminescence lifetimes and intensities in Figure 3 reveals effects that could arise from the population of different levels separated by less than 100 cm^{-1}, qualitatively supporting our assignment. Spin−orbit coupling constants ζ of 500 and 900 cm^{-1} were used for K_2PdBr_4 and K_2PdCl_4, respectively, to calculate the energies of the ligand-field states in Table 1.

Table 1. Energies of the Electronic States for K_2PdBr_4 and K_2PdCl_4[a]

	energy, cm^{-1}			
	K_2PdBr_4		K_2PdCl_4	
state	calcd	obsd	calcd	obsd
$^1A_{1g}$				
Γ_1	0		0	
^3E_g				
Γ_1	14 452		14 456	
Γ_2	14 506		14 635	
Γ_5	14 637	14 645[b]	14 754	14 800[b]
Γ_4	14 835		15 093	
Γ_3	14 992		15 491	
$^3A_{2g}$				
Γ_5	15 981	16 035[b]	16 158	17 005[b]
Γ_1	16 071		16 444	17 000[d]
$^3B_{1g}$				
Γ_5	16 842	17 420[b]	17 614	17 700[d]
Γ_4	16 980	17 000,[c] 17 400[c] 16 960,[d] 17 400[d]	17 997	17 700[e]
$^1A_{2g}$				
Γ_2	20 369	20 200[c] 20 200[d]	20 915	21 700[d] 21 000[e]
^1E_g				
Γ_5	22 410	21 800[c] 22 100[d]	23 356	23 200[d] 22 500,[e] 23 300[e]
$^1B_{1g}$				
Γ_3	25 463	27 100[c] 26 990[d]	26 719	28 500[e]

[a] K_2PdBr_4: $e_\sigma = e'_\sigma = 9900$ cm^{-1}, $e_{\pi\perp} = e_{\pi\parallel} = 1800$ cm^{-1}, $a = a_0 = b = 0$; $B = 530$ cm^{-1}, $C = 2200$ cm^{-1}; $\zeta = 500$ cm^{-1}. K_2PdCl_4: $e_\sigma = e'_\sigma = 10\,340$ cm^{-1}, $e_{\pi\perp} = e_{\pi\parallel} = 1980$ cm^{-1}, $a = a_0 = b = 0$; $B = 540$ cm^{-1}, $C = 2400$ cm^{-1}; $\zeta = 900$ cm^{-1}. [b] This work. [c] Reference 8. [d] Reference 19. [e] Reference 18.

Vibronic Intensity Mechanism for the Lowest Energy Transition. It was shown in a series of theoretical studies on tetrahaloplatinates that low-frequency ungerade parity modes account for the total electric dipole intensity of parity forbidden transitions in these systems.[7,16] High-frequency ungerade stretching modes can be neglected as enabling modes.[7,16] We apply these results to the title compounds. The vibrational energies of the low-frequency modes for K_2PdBr_4 are 85 (e_u, lattice), 100 (a_{2u}, lattice), 130 (e_u, bending), and 140 cm^{-1} (a_{2u}, bending).[40] The electronic origin of K_2PdBr_4 is therefore expected to be hidden at the beginning of the onset to the luminescence peak at 12 525 cm^{-1}, with an experimental width of more than 100 cm^{-1}. This peak corresponds most likely to a superposition of several vibronic origins involving low-frequency enabling modes, and we denote it as the apparent origin in the analysis presented in the following section. Vibronic selection rules are given in Table 2 of ref 8 and indicate that low-frequency enabling modes lead to allowed $^1A_{1g} \leftrightarrow {}^3E_g$ transitions in both E ∥ c and E ⊥ c polarizations, in agreement

(32) Griffith, J. S. *The Theory of Transition Metal Ions*; University Press: Cambridge, 1961.
(33) Ferguson, J. *Prog. Inorg. Chem.* **1970**, *12*, 159.
(34) Riesen, H.; Krausz, E. R.; Dubicki, L. *J. Lumin.* **1989**, *44*, 97.
(35) Zink, J. I. *J. Chem. Soc., Dalton Trans.* **1996**, 4027.
(36) Ham, F. S. *Phys. Rev.* **1965**, *138*, A1727.
(37) Sturge, M. D. *Solid. State Phys.* **1967**, *20*, 91.
(38) Wilson, R. B.; Solomon, E. I. *Inorg. Chem.* **1978**, *17*, 1729.
(39) Güdel, H. U.; Snellgrove, T. R. *Inorg. Chem.* **1978**, *17*, 1617.
(40) Perry, C. H.; Athans, D. P.; Young, E. F.; Durig, J. R.; Mitchell, B. R. *Spectrochim. Acta* **1967**, *23A*, 1137.

Table 2. Spectroscopic parameters for K_2PdBr_4 and K_2PdCl_4

parameter	K_2PdBr_4	K_2PdCl_4
gs vib energy		
$k_{a_{1g}}$ (cm^{-1})[a]	187.4	303.6
$k_{b_{1g}}$ (cm^{-1})[a]	166.6	269.9
es vib energy		
$k_{a_{1g}}$ (cm^{-1})[b]	211.0	303.6
$k_{b_{1g}}$ (cm^{-1})[b]	180.0	269.9
Stokes shift (cm^{-1})	3420	3865
E_{00} (cm^{-1})[c]	12 525	12 735
$\Delta_{a_{1g}}{}^{b}{}_{b,d}$	3.90	3.68
$\Delta_{b_{1g}}{}^{e}$	1.73	1.18
$\Delta_{b_{1g}}{}^{f}$	1.25	0.70
V_{12} (cm^{-1})[b]	0.89	0.57
Γ (cm^{-1})[b]	400	300
energy barrier (cm^{-1})[e]	42	108
	28	8

[a] From Raman spectra.[27] [b] Fit parameters for calculated spectra. [c] From luminescence spectra. [d] From minima of diabatic potentials. [e] From minima and maximum of the lower adiabatic potential. [f] From maxima of emitting-state eigenfunction in Figure 4b.

with our absorption spectra, where the lowest-energy band is observed in both polarizations. Progressions in totally symmetric and Jahn−Teller active modes built on different vibronic origins are expected to be identical, but shifted by the energy difference of the enabling modes.[38,39] A superposition of such progressions is not sufficient to rationalize the changing shapes of the clusters of peaks forming the main progression across the luminescence spectrum in Figure 1. A model to interpret the vibronic structure is presented in the following section.

Vibronic Structure in the Luminescence Spectra. The luminescence and absorption spectra of the title compounds in Figures 1 and 2 allow us to determine the normal coordinates along which bond length changes in the emitting state occur. We concentrate on K_2PdBr_4 for our analysis because its spectra show better resolution than K_2PdCl_4. The approach is the same for both systems, and numerical values for all parameters of our model are compiled in Table 2.

The main progression built on the apparent origin at 12 525 cm^{-1} in the luminescence spectrum is in the totally symmetrical a_{1g} mode, with a vibrational frequency of 187.4 cm^{-1} determined from the Raman spectrum of K_2PdBr_4.[27] The long progression indicates a large structural change between the ground and emitting states along the totally symmetrical normal coordinate. Each peak in the luminescence spectrum shown in Figure 5 has at least two shoulders corresponding to distortions along another normal coordinate. On the basis of the energy difference between maxima and shoulders, we assign the second normal mode as the non-totally symmetrical in-plane b_{1g} vibration with a frequency of 166.6 cm^{-1}.[27] The presence of vibronic structure involving a non-totally symmetrical vibrational mode of gerade parity is experimental evidence for a Jahn−Teller effect, making the title compounds rare representatives of square-planar molecules with resolved spectra documenting an $E_g \times b_{1g}$ Jahn−Teller effect in the emitting state.[37,41]

We use harmonic potential energy surfaces as a function of the normal coordinates $Q_{a_{1g}}$ and $Q_{b_{1g}}$ to represent the initial and final states of the electronic transitions. These simple surfaces are described by a small number of parameters and are illustrated in Figure 4. Two potential energy surfaces displaced by $\pm\Delta_{b_{1g}}$ are required to define the emitting state along the normal coordinate $Q_{b_{1g}}$. This is an approximation to the manifold of levels arising from ^3E_g by spin−orbit coupling, as listed in Table 1. The spectroscopic results do not allow us to determine

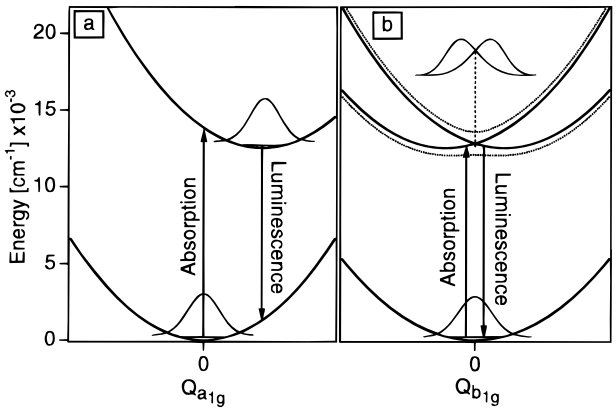

Figure 4. Potential energy surfaces describing the low-energy luminescence and absorption transitions: (a) totally symmetrical a_{1g} normal coordinate; (b) non-totally symmetrical b_{1g} normal coordinate. The lowest eigenfunctions are shown on the ground- and excited-state surfaces. Electronic transitions are indicated by arrows. The excited-state eigenfunction in b is offset along the ordinate for clarity, as indicated by the dashed line. Diabatic potentials are shown as solid lines, adiabatic potentials as dotted lines.

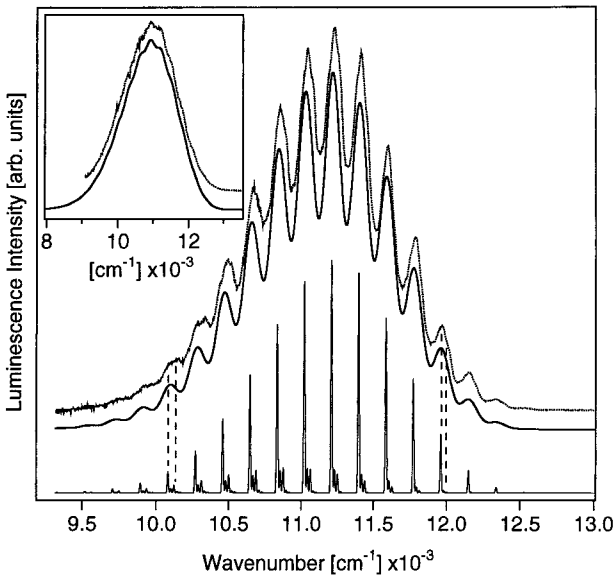

Figure 5. Calculated and experimental luminescence spectra of K_2PdBr_4 (main figure) and K_2PdCl_4 (inset). Experimental spectra are shown as dotted lines; solid lines denote the calculated spectra. Best-fit spectra are calculated with the parameters from Table 2; highly resolved spectra are calculated with $\Gamma = 3$ cm^{-1} and all other parameters from Table 2.

independent parameters for each level. It is interesting to note that, in organic cumulenes with D_{2d} symmetry, vibronic structure arising from non-totally symmetrical modes is observed even for formally nondegenerate levels, if a nearby level is degenerate.[41] According to the ligand-field analysis in Table 1, the lowest levels are nondegenerate for both title compounds, and the spectra of K_2PdCl_4 and K_2PdBr_4 possibly show an effect similar to ref 41. A further simplification in our model is the limitation to only one non-totally symmetrical mode: in D_{4h} symmetry, distortions along a second non-totally symmetrical vibration of b_{2g} symmetry are possible,[41] but our spectra do not show vibronic peaks corresponding to an additional vibrational mode. One effect resulting from an additional mode was included in our model as shown in Figure 4b of ref 41 by allowing a coupling between the two surfaces along the b_{1g} coordinate, leading to the potential energy surfaces for the ground and emitting states illustrated in Figure 4b.

The potential energy surface of the final state of the electronic

(41) Cederbaum, L. S.; Domcke, W.; Köppel, H. *Chem. Phys.* **1978**, *33*, 319.

transition along a dimensionless normal coordinate Q_i is defined by its harmonic frequency k_i in cm^{-1}. The minimum of the ground-state potential energy surface is at the origin of the normal coordinate system in Figure 4, and the excited-state potential minima are at Δ_i. We include a coupling constant V_{12} in cm^{-1} along the b_{1g} normal coordinate for the degenerate ^3E_g state. The excited-state potentials $V_{a_{1g}}$ and $V_{b_{1g}}$ are obtained with eqs 1 and 2, as illustrated in Figure 4:

$$V_{a_{1g}} = {}^1/_2 k_{a_{1g}}(Q_{a_{1g}} - \Delta_{a_{1g}})^2 \quad (1)$$

$$V_{b_{1g}} = \begin{pmatrix} {}^1/_2 k_{b_{1g}}(Q_{b_{1g}} - \Delta_{b_{1g}})^2 & V_{12} \\ V_{12} & {}^1/_2 k_{b_{1g}}(Q_{b_{1g}} + \Delta_{b_{1g}})^2 \end{pmatrix} \quad (2)$$

Before the electronic transition, the system is described by the lowest energy eigenfunction of the initial electronic state. Harmonic oscillator functions with the parameters in Table 2 were used for all calculations, with the exception of the excited state along the b_{1g} coordinate in Figure 4b. This function is calculated numerically and is included in Figure 4b.[42,43]

We use the time-dependent theory of electronic spectroscopy to calculate absorption and luminescence spectra. Its application to transition metal compounds has been discussed in detail previously.[15,44,45] Electronic absorption and luminescence spectra are given by[46,47]

$$I(\omega) = \omega^c \int_{-\infty}^{+\infty} e^{i\omega t}\{\langle\phi|\phi(t)\rangle e^{-\Gamma^2 t^2 + iE_{00}t/\hbar}\}\, dt \quad (3)$$

with $I(\omega)$ denoting the intensity in arbitrary units at frequency ω, E_{00} the energy of the apparent origin, and Γ a phenomenological damping factor, determined from the width of each band forming the vibronic structure. The exponent c has a value of 1 or 3 for absorption or luminescence spectra.

The most important ingredient to eq 3 is $\langle\phi|\phi(t)\rangle$, the autocorrelation function of a wavepacket ϕ prepared on the potential energy surface of the final state during the electronic transition. We assume transition dipole moments that are constant along the a_{1g} and b_{1g} coordinates, and therefore ϕ is identical in shape to the eigenfunction describing the system before the transition. The time-dependent wavefunction $\phi(t)$ is obtained with a split-operator algorithm[42,43] for both degenerate and nondegenerate electronic states. The calculation of emission spectra involving degenerate excited states and a nondegenerate ground state was discussed previously.[45] The autocorrelations of the orthogonal a_{1g} and b_{1g} normal coordinates are multiplied, and the product is Fourier-transformed to the frequency domain to obtain a calculated spectrum.

Figure 5 shows the experimental and calculated luminescence spectra of K_2PdBr_4 and K_2PdCl_4. All parameters for the theoretical model are summarized in Table 2. Numerical values for $\Delta_{a_{1g}}$, $\Delta_{b_{1g}}$, $k_{a_{1g}}$ (emitting state, es), and $k_{b_{1g}}$ (es) are obtained from the adjustment of the calculated spectra to the experimental data. The agreement between experimental and calculated spectra is good for both compounds, especially in view of the simplified potential energy surfaces used for the ^3E_g state, a likely reason for some discrepancies in the intensities of vibronic shoulders. The positions of the shoulders and the relative shapes of the vibronic peaks across the spectrum are well represented by our model, as indicated for two examples by the dotted vertical lines in Figure 5.

The harmonic vibrational frequency $k_{b_{1g}}$ (es) appears to be higher than the ground-state value. The true vibrational frequency is given by the energy difference between the two lowest eigenvalues of the coupled surfaces in Figure 4b. This value is 155 cm^{-1}, lower than the ground-state vibrational energy. We obtain the best agreement between calculated and experimental spectra for a value of $k_{a_{1g}}$ (es) that is higher than in the ground state, again possibly caused by our simplified potential energy surfaces. Holding $k_{a_{1g}}$ (es) fixed at the ground-state value of 187.4 cm^{-1} does lead to a somewhat inferior, but acceptable fit with a value of 3.93 for $\Delta_{a_{1g}}$, differing by less than 1% from the result in Table 2. The calculated luminescence spectra are not very sensitive to the numerical value of the coupling constant V_{12}, and satisfactory fits are obtained for values ranging from 0 to 600 cm^{-1}. The luminescence spectrum for K_2PdCl_4 has less resolved structure, but its analysis leads to similar distortions, confirming a small but nonzero contribution from the b_{1g} mode to both spectra. We have also calculated emission spectra based on an apparent origin at 12 712 cm^{-1} ($E_{00} + k_{a_{1g}}$ (gs)), a model where the apparent origin is too weak to be observed. This model leads to a somewhat inferior fit with a $\Delta_{a_{1g}}$ larger by 7% than the value in Table 2 but also requires a value of $k_{a_{1g}}$ (es) of 230 cm^{-1}, an even higher increase from the ground state than the value in Table 2. The positions of the potential energy minima are therefore only weakly affected by these details of the excited-state potential energy surfaces.

A change of $\Delta_{b_{1g}}$ by 10% leads to a calculated luminescence spectrum inferior to the fit shown in Figure 5. We can exclude a large value of $\Delta_{b_{1g}}$ based on the spacing of the main progression in the luminescence spectra of K_2PdBr_4 and K_2PtCl_4.[28] In the palladate, the spacing is identical within experimental accuracy to the a_{1g} mode, indicating that bond length changes occur mainly along this totally symmetric normal coordinate, whereas in the platinate the members of the main progression are separated by 315 cm^{-1}, indicating comparable contributions from the a_{1g} (329 cm^{-1}) and b_{1g} (304 cm^{-1}) modes.[28]

We have tested alternative models for K_2PdBr_4 containing only the totally symmetrical a_{1g} mode, or the a_{1g} mode combined with a low-frequency mode, corresponding to a lattice vibration. The resulting best fit was inferior to the result obtained in Figure 5 with the a_{1g} and b_{1g} molecular modes of the square-planar $[PdX_4]^{2-}$ unit.

The Energy Gap. The quantitative model for the potential energy surfaces of the ground and emitting states obtained from the analysis of the luminescence spectra should allow us to calculate the shape of the lowest energy absorption band. Experimental and calculated luminescence and absorption spectra of K_2PdBr_4 using the parameters in Table 2 are shown in Figure 6. The calculated absorption spectra with zero coupling and with a coupling V_{12} of 400 cm^{-1} are represented as dashed and solid lines, respectively. The band calculated with $V_{12} = 0$ has its maximum at an energy lower by approximately 800 cm^{-1} than the experimental spectrum. The calculation with nonzero coupling leads to a much better agreement, although it predicts somewhat higher intensities in the region of the energy gap than observed, most likely another consequence of our simplified potential energy surfaces. The calculated absorption band clearly identifies the very lowest observed band as the counterpart to the emission spectrum and defines the numerical value of the coupling constant V_{12} as 400 cm^{-1}.

(42) Feit, M. D.; Fleck, J. A.; Steiger, A. *J. Comput. Phys.* **1982**, *47*, 412.
(43) Kosloff, D.; Kosloff, R. *J. Comput. Phys.* **1983**, *52*, 35.
(44) Reber, C.; Zink, J. I. *Comments Inorg. Chem.* **1992**, *13*, 177.
(45) Wexler, D.; Zink, J. I.; Reber, C. *J. Phys. Chem.* **1992**, *96*, 8757.
(46) Heller, E. J. *J. Chem. Phys.* **1975**, *62*, 1544.
(47) Heller, E. J. *Acc. Chem. Res.* **1981**, *14*, 368.

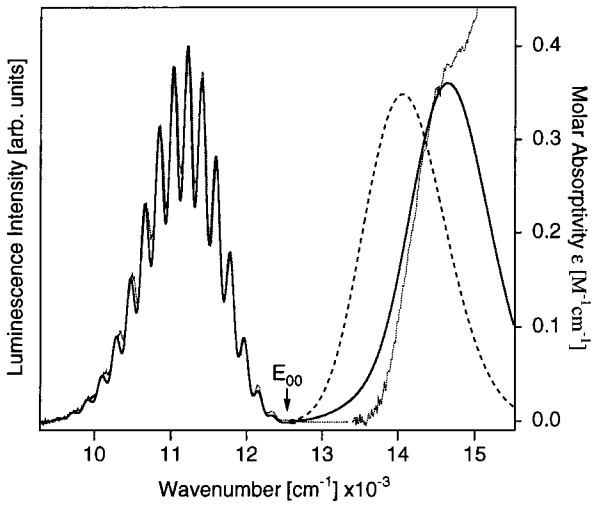

Figure 6. Calculated and experimental luminescence and absorption spectra of K_2PdBr_4. Experimental spectra are shown as dotted lines, solid lines denote the best-fit calculated luminescence and absorption spectra obtained with the parameters in Table 2. The dashed line shows the calculated absorption spectrum with $V_{12} = 0$ cm^{-1} and all other parameters from Table 2.

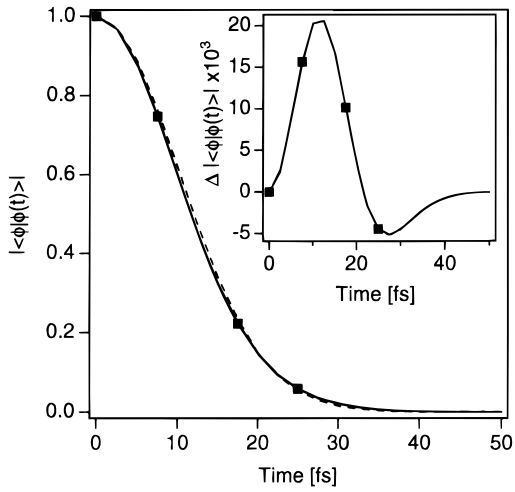

Figure 7. Autocorrelation functions used to calculate the absorption spectra of K_2PdBr_4 in Figure 6. The autocorrelation for the model with $V_{12} = 0$ is indicated by the dotted line; the solid line denotes the autocorrelation calculated with a coupling constant V_{12} of 400 cm^{-1}. Solid squares indicate the times for which time-dependent wavefunctions are shown in Figure 8. The difference between the autocorrelation functions in the main figure is shown in the inset.

Vibronic origins displaced by one quantum of an ungerade parity enabling mode from the electronic origin lead to a gap of twice the vibrational energy of the low-energy ungerade parity enabling modes. This effect shifts the calculated absorption bands to higher energy by less than 200 cm^{-1}, which can be accounted for in our model by a higher energy of the apparent origin E_{00} for absorption than for luminescence combined with a smaller coupling constant V_{12}. The value in Table 2 therefore defines an upper limit for V_{12}, which could be lowered by a maximum of 100 cm^{-1} because of the vibronic origins. Even the highest frequency mode of ungerade parity, the e_u stretching mode with a vibrational energy of 260 cm^{-1},[40] is not sufficient to rationalize the entire energy gap for K_2PdBr_4.

Time-dependent theory allows us to visualize the effects caused by coupling between the potential energy surfaces along the b_{1g} coordinate and also to compare in more detail the emitting states of the title compounds to those of the platinum analogs. The autocorrelation functions $\langle\phi|\phi(t)\rangle$ used to calculate the absorption spectra in Figure 6 are presented in Figure 7 for K_2PdBr_4 at short times. The inset to Figure 7 shows the calculated difference between the autocorrelation functions obtained with $V_{12} = 0$ and $V_{12} = 400$ cm^{-1}. These functions include both the a_{1g} and b_{1g} coordinates, but the wavepacket dynamics along the a_{1g} coordinate is not influenced by V_{12}. In the following we examine the time evolution of the wavefunction along the b_{1g} coordinate at the times indicated by the solid squares in Figure 7.

Figure 8 shows the time-dependent wavefunction on the surfaces along the b_{1g} coordinate for values of 400 (solid lines) and 0 cm^{-1} (dotted lines). At 7.5 fs, the maximum of the wavepacket moving on the coupled surfaces is further away from the initial position than the function on the uncoupled potentials. This trend continues at 17.5 fs, and it causes the steeper initial decrease of the autocorrelation function for nonzero coupling, illustrated by the solid line in Figure 7 and leading to the positive difference in the inset to Figure 7. On the coupled surfaces, components of the wavepacket can move toward both minima of the potential well, whereas the whole wavepacket moves toward only one potential energy minimum on uncoupled surfaces. This effect is observed in the low-amplitude regions at the leading and trailing edges of the wavepacket: the part of the function that starts out near the

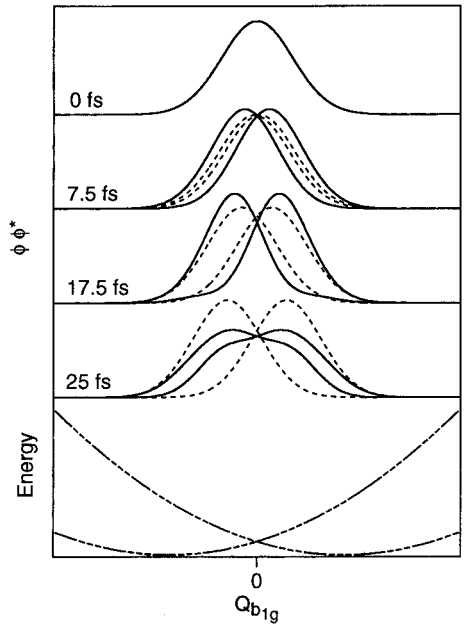

Figure 8. The evolution of the time-dependent wavefunction on the b_{1g} surfaces with $V_{12} = 400$ cm^{-1} (solid lines) and $V_{12} = 0$ (dotted lines). The times represented are indicated by solid symbols in Figure 7. The potential energy surfaces for $V_{12} = 0$ are included at the bottom of the figure.

potential minima moves in a very similar way on coupled and uncoupled surfaces. Large differences are clearly visible in the region near $Q_{b_{1g}}$=0 at 17.5 fs, and these differences lead to the steep initial decrease of the autocorrelation, shown as a solid line in Figure 7. The absorption spectrum arising from the coupled surfaces therefore has its maximum further away from the electronic origin,[47] as illustrated in Figure 6.

Qualitatively similar short-time wavepacket dynamics within a simpler model, consisting of the double-minimum (lower adiabatic) potential energy surface only, reproduces the energy gap for K_2PtCl_4.[15,28] This model leads to a calculated absorption band shape that depends strongly on the ratio between the width of the wavepacket at $t = 0$ and the width of the energy barrier of the double-minimum potential and would lead to much higher

absorbances in the region of the energy gap than observed for K_2PdBr_4.

We notice a similar width at half-height and overall shape in the region of the band maximum of the two calculated absorption spectra in Figure 6. This similarity is a consequence of the amplitude transfer between coupled surfaces and cannot be obtained from the model containing the lower double-minimum surface only. At 25 fs, the amplitude transfer leads to very large wavepackets, delocalized over the entire region between the potential energy minima in Figure 8 and greatly reducing the difference between the autocorrelation functions shown in the inset to Figure 7. The small difference between the autocorrelation functions at times longer than 25 fs leads to small changes in vibronic spacings of the intense regions of the absorption spectra and accounts for the similar band shapes in Figure 6, illustrating the importance of explicitly including two coupled excited-state surfaces for the title compounds.

The Emitting-State Geometry. We determine the lowest energy excited-state geometry from the model parameters in Table 2. The dimensionless displacements Δ_i along the normal coordinates Q_i are first converted to ΔQ_i in angstroms.[48] The relationships between the displacement ΔQ_i and the Pd−X (X = Cl, Br) bond length changes δr(Pd−X) in angstroms are[28]

$$\Delta Q_{a_{1g}} = {}^1/_2[\delta r(\text{Pd}-\text{X})_1 + \delta r(\text{Pd}-\text{X})_2 + \delta r(\text{Pd}-\text{X})_3 + \delta r(\text{Pd}-\text{X})_4] \quad (4)$$

$$\Delta Q_{b_{1g}} = {}^1/_2[\delta r(\text{Pd}-\text{X})_1 - \delta r(\text{Pd}-\text{X})_2 + \delta r(\text{Pd}-\text{X})_3 - \delta r(\text{Pd}-\text{X})_4] \quad (5)$$

In the vast majority of the existing literature, excited-state bond length changes in transition metal compounds are determined from the positions of the minima of multidimensional harmonic potential energy surfaces.[48] This approach is no longer valid for coupled potentials, where the minima of the harmonic (diabatic) surfaces are not a good measure for the structural changes. To a first approximation, the positions of the minima of the lower adiabatic surface along the b_{1g} coordinate can be used to determine $\Delta_{b_{1g}}$. These values are smaller by 28% and 40% than those from the harmonic minima for K_2PdBr_4 and K_2PdCl_4, respectively. A more accurate measure for $\Delta_{b_{1g}}$ is obtained from the maximum of the squared eigenfunction of the lowest energy excited vibronic level, shown in Figure 5 for K_2PdBr_4 and leading to values smaller by 49% and 52% for K_2PdBr_4 and K_2PdCl_4, respectively. These values take into account the significant delocalization of the system across the shallow energy barrier separating the two electronic states, leading to the rapid dynamics illustrated in Figure 8.[38,39] The small non-totally symmetrical structural distortions in the title compounds nevertheless influence the optical spectra significantly.

The bond length changes δr(Pd−X) from eqs 4 and 5 are 0.12 Å for one pair of opposite halide ions in both K_2PdCl_4 and K_2PdBr_4 and 0.09 and 0.07 Å for each of the other pair of Pd−X bonds in K_2PdCl_4 and K_2PdBr_4, respectively. We estimate errors of 1 unit in the last digits of the bond length changes. These distortions correspond to changes of less than 5% of the ground-state bond lengths.[22,23] The deviation from D_{4h} symmetry in the ^3E_g excited state is smaller for K_2PdCl_4 than for its platinum analog. In K_2PtCl_4, the bond length increases for one pair of Pt−Cl bonds by 0.14 Å, and for the other pair it decreases by 0.02 Å, a consequence of the much larger distortion along the b_{1g} coordinate.[15,28] This large difference of the excited-state distortions is remarkable, considering the identical overall crystal structure, leading to metal−chloride bond lengths that differ by only 0.1%[22] and metal−metal distances between square-planar chromophores that differ by only 0.8%,[22] as well as in view of the identical orbital character of the lowest energy electronic transition.

The barrier heights of the lower adiabatic potential, shown schematically in Figure 4, are 28 and 8 cm^{-1} for K_2PdBr_4 and K_2PdCl_4, respectively. These barriers are lower by orders of magnitude than those for K_2PtCl_4, where a value of 3000 cm^{-1} was determined from the double-minimum surface along the b_{1g} coordinate.[15] The lower energy barrier is related to the smaller non-totally symmetrical distortion, the most important difference between the first excited states of tetrahalopalladates and tetrahaloplatinates.

In summary, we have characterized the lowest energy excited state of both K_2PdCl_4 and K_2PdBr_4 by combining detailed spectroscopic measurements with theoretical models. Near-infrared luminescence spectra show vibronic structure involving the totally symmetrical a_{1g} and the Jahn−Teller active b_{1g} vibrational modes. The energy gap between absorption and luminescence spectra is a consequence of distortions along non-totally symmetrical modes in the lowest energy excited state of the title compounds.

Acknowledgment. This work was made possible by research grants from the NSERC (Canada) and FCAR (Province of Quebec). Y.P. acknowledges FCAR for a graduate research fellowship.

Supporting Information Available: Table of the matrix elements used for the ligand-field calculation in Table 1 (2 pages). Ordering information is given on any current masthead page.

IC960388S

(48) Zink, J. I.; Kim Shin, K.-S. In *Advances in Photochemistry*; Volman, D. H., Hammond, G. S., Neckers, D. C., Eds.; John Wiley: New York, 1991; Vol. 16; p 119. The relation between dimensionless values Δ_i and ΔQ_i in Å is $\Delta_i = (Nh/(4\pi^2 c\omega_i m_i))^{1/2}\Delta Q_i \times 10^8$ Å/cm, where N is Avogadro's number, h is Planck's constant in g cm^2 s^{-1}, c is the speed of light in cm s^{-1}, ω_i is the frequency of vibrational mode i in cm^{-1}, and m_i is the mass for mode i in gram/mol. Masses of 35.453 and 79.904 g/mol were used for the a_{1g} and b_{1g} modes of the title compounds.